ON SIMULATING THE ATMOSPHERIC BOUNDARY LAYER IN WIND TUNNELS

N J Cook, BSc(Eng), PhD, FRMetS

Two papers reprinted from *Journal of Industrial Aerodynamics,* 1978, 3 (2/3) 157–176, and 2 (4) 311–321

1 Wind-tunnel simulation of the adiabatic atmospheric boundary layer by roughness, barrier and mixing-device methods

The philosophy of roughness, barrier and mixing-device simulation methods is discussed. The functions of the various physical components are illustrated by measurements of simulations in the BRE Boundary Layer Wind Tunnel and their performance is evaluated.

It is concluded that boundary layers grown entirely naturally over a long fetch of roughness give the best simulations and that the artificial thickening by barrier and mixing-device, required to produce smaller scale factors, inevitably reduces the quality of the simulation. The paper goes some way towards quantifying the degree of 'artificiality' thus introduced.

2 Determination of the model scale factor in wind-tunnel simulations of the adiabatic atmospheric boundary layer

A process is proposed for determining the model scale factor in contemporary full-depth or part-depth simulations of the atmospheric boundary layer in a wind tunnel.

Building Research Establishment
Building Research Station
Garston
Watford
WD2 7JR

Journal of Industrial Aerodynamics, 3 (1978) 157—176

WIND-TUNNEL SIMULATION OF THE ADIABATIC ATMOSPHERIC BOUNDARY LAYER BY ROUGHNESS, BARRIER AND MIXING-DEVICE METHODS*

N.J. COOK

Department of the Environment, Building Research Establishment, Garston, Watford WD2 7JR Herts. (Gt. Britain)

Summary

The philosophy of roughness, barrier and mixing-device simulation methods is discussed. The functions of the various physical components are illustrated by measurements of simulations in the BRE Boundary Layer Wind Tunnel and their performance is evaluated.

It is concluded that boundary layers grown entirely naturally over a long fetch of roughness give the best simulations and that the artificial thickening by barrier and mixing-device, required to produce smaller scale factors, inevitably reduces the quality of the simulation. The paper goes some way towards quantifying the degree of 'artificiality' thus introduced.

1. Introduction

The problems of simulating the atmospheric boundary layer in wind tunnels have been reviewed by Davenport and Isyumov [1] and by Cermak and Arya [2]. Both sources concluded that the boundary layer which grows naturally on a long rough wall is a good model of the adiabatic atmospheric boundary layer in terms of both the mean and the turbulent velocity characteristics and is superior to artificial methods, involving grids of rods, plates, vortex generators, etc., in which the turbulence characteristics (if simulated at all) decay downstream. The atmospheric boundary layer can be considered as adiabatic in winds stronger than about 10 m/s, when thermal effects are swamped by the strong mechanically generated turbulence; thus an adiabatic simulation is more applicable to wind loading or environmental safety studies in strong winds than, for example, to effluent dispersal studies. The simulation of unstable or stable stratified flows is practicable in a wind tunnel, but requires complex techniques and equipment for heating and cooling the air. A Meteorological wind tunnel with these facilities at Colorado State University has been described by Cermak and Arya [2].

Once a natural rough-wall boundary layer has been adopted as a good model, the major problem is that of generating a layer of sufficient depth in the available wind-tunnel length. With a length of almost 25 m, the Boundary Layer Wind Tunnel at the University of Western Ontario is among the longest constructed, yet boundary layer depths of only 900 mm over simulated urban roughness (25—100 mm high blocks) and 380 mm over simulated rural terrain (carpet) were obtained naturally [1], resulting in approximate linear scales of 1/400 and 1/1000 respectively. Deeper boundary layers were obtained by inserting a 300-mm-high grid of rods upstream of the roughness to give the boundary layer an 'artificial' start. Davenport and Isyumov [1] concluded that the resulting boundary layer was adequate,

but a complete assessment of its accuracy was not possible at that time (1967) until information on the crosswind and vertical components of turbulence and the higher-order correlations in full scale became available.

In the decade since then, full-scale measurements have increased the data on the atmospheric boundary layer to the stage that ESDU [3,4] and Counihan [5] have been able to collate the data and present them on a parametric basis. Recently, Deaves and Harris [6] have proposed a mathematical model for strong winds based on a modified form of the Asymptotic Similarity Theory and requiring only one closure assumption. When examined closely, the experimental and theoretical results differ slightly in form but agree in value to within a few per cent over the lower 200 m. Simulation techniques kept pace with the accumulation of full-scale data and the range of methods currently available was summarised by Hunt and Fernholz [7] in their report on the 50th Euromech colloquium on simulations. The naturally grown boundary layer gives excellent agreement with the atmospheric data, but is restricted to those research institutions that can justify the expense of a very long wind tunnel. Purely artificial techniques in short wind tunnels, based on the original approaches by Owen and Zienciewicz [8] with graded grids or by Elder [9] with curved screens, in which only the mean velocity profile is represented, still have their place, but their usefulness is confined to mean velocity measurements in the near field of buildings. The majority of contemporary simulation methods are a compromise between the previous two extremes, in which a natural boundary layer is allowed to develop over an intermediate length of roughened wall after an initial artificial start, and may be described by the general classification of 'roughness, barrier and mixing-device methods'.

2. Roughness, barrier and mixing-device methods

If the experience of the author can be regarded as typical, selection of the various physical components or 'hardware' for the different methods was largely made on the basis of intuition and trial-and-error. As a result, the hardware differs considerably in form between methods, for example between the methods of Counihan [10,11], Standen [12] and Cook [13], but performs substantially the same role. The role of the surface roughness is the same as in a naturally grown layer; it represents the roughness of the full-scale ground surface and, acting as a momentum sink, establishes a profile of Reynolds stress through the layer which in turn controls the mean velocity profile and turbulence characteristics. The surface roughness is the most important component, in that it establishes the values of the three 'law-of-the-wall' parameters z_0, d and u_*. The barrier and the mixing-device are the 'artificial' part of the simulation. The role of the barrier is to give an initial momentum deficit and depth to the layer which is mixed into the developing layer by turbulence generated by the mixing-device. The flow is tricked by the barrier into believing the fetch of roughness to be longer, and by the mixing-device that the barrier is not there at all! In the ideal case, the flow in the test area near the downstream end of the surface roughness should have the characteristics of a boundary layer grown naturally over a much longer fetch of the same surface roughness, without any additional characteristics imposed by the barrier or mixing-device. The intended role of the barrier is therefore to establish the boundary-layer height h.

There is often interaction between the barrier and the mixing-device. Counihan [10,11] placed his barrier (initially a plane wall) upstream of the mixing-device (a row of 'elliptic wedge' vorticity generators) but found that the momentum deficit of the wall was reduced on the centre-line of each vorticity generator by the strong turbulent mixing. His solution was to increase locally the height of the wall immediately upstream of each vorticity generator, resulting in a castellated wall. Cook [13] placed his barrier (again initially a plane wall) downstream of the mixing-device (a square mesh grid) but found that the wall could be made to assist the mixing by adding perforations near the top. As a contrast, Standen [12] was able to combine the

barrier and mixing-device into one component, a row of tapering spires. (The consequences of not attempting to represent the full-depth of the boundary layer, as in Cook's method [13], will be discussed later, in the light of the results presented in this paper.)

Although comparison of the two Counihan methods [10,11] with the earlier method by Armitt and Counihan [14] and with later measurements [15,16] gives a fascinating insight into the development methodology, each stage was presented as a completed work for a particular application, i.e. 'rural' and 'urban' simulations. The 'urban' method of Cook [13] was presented in the same manner. Only Standen [12] proposed his spires as being useful components for producing a family of simulations for different terrains. Knowledge of the sensitivity of the final simulation to changes in size and form of the various hardware components would be very useful. This paper will attempt to quantify the sensitivity by evaluating the methods and facilities currently in use at the Building Research Establishment.

The scope of this paper is confined to 'passive' methods of the type already described. There has been a recent trend [7] to 'active' methods in which the physical barrier is replaced by air-jets, and the mixing-device may be omitted altogether. The major advantage claimed for these methods is that the momentum deficit can be adjusted independently of the windspeed. There are, however, claims which are not well founded. For example, the claim by Nagib et al. [17] that their counter-jet technique introduces only small length scales of the order of the jet diameters and spacings can be disputed on the grounds that the separation bubble which is formed has the same characteristic length scales as if the bubble were produced by a solid barrier; and this will also apply to other similarly based systems. A common claim, that the active systems allow independent adjustment of mean velocity and turbulence characteristics [7], raises two points. Firstly, this can also be achieved passively, by variations in the form of barrier or mixing-device, if required. Secondly, and more importantly, it is an admission that these active devices are, in some cases, permitted to control the flow characteristics to the extent of excluding the influence of the surface roughness, resulting in a simulation which is more 'artificial' than 'natural'. From a personal viewpoint, the advantages and disadvantages of active and passive methods seem to be evenly balanced. In wind tunnels with large cross-sections, where changing hardware for different applications is a major construction exercise, the expense of installing active devices may be justified. In smaller wind tunnels, where provision has been made for the easy insertion of flow devices [18,19], passive barriers and mixing-devices are adequate.

3. Apparatus and techniques

All measurements were made in the 2-m-wide by 1-m-high BRE Boundary Layer Wind Tunnel, described in this journal by Cook [19]. Over the period of the measurements (January 1976 to June 1977) the wind tunnel was moved from its initial position (across the width of the laboratory) and aligned parallel to the long axis of the building. This allowed the original working-section length of 8 m to be increased in stages to the present 14 m by the insertion of 6 m of plain working section between the 'flow processing section' [19] at the upstream end and the glazed test area at the downstream end. The tunnel was run near the middle of its speed range. A reference windspeed in the test area of 10 m/s at 750 mm above the floor was maintained, monitored by a Pitot-static tube and Betz manometer.

A typical arrangement of simulation hardware is shown with dimensions in Fig. 1, which illustrates a refinement of the method evolved at Bristol University by Cook [13]. The additional fetch of roughness available allowed a coarser-mesh grid to be used, producing a larger scale of turbulence. Also, the use of a smaller slat width reduced the pressure drop (and thus the power requirement of the tunnel) without a significant drop in generated turbulence intensity. Where this turbulence grid was used it is designated GRID in the figure captions; otherwise a plain gauze with a

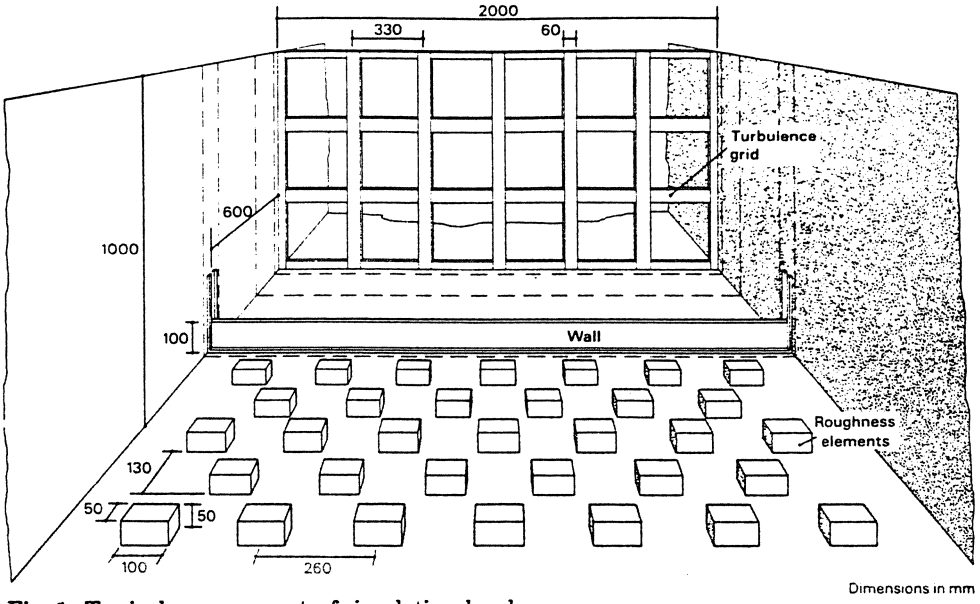

Fig. 1. Typical arrangement of simulation hardware.

resistance coefficient of 1.6 was inserted in its place to give a free-stream turbulence intensity less than 0.5%. Two arrays of 'elliptic wedge vorticity generators' of the Counihan type were also used. Designated by their heights as 400 mm COUNIHAN and 800 mm COUNIHAN, their proportions and spacings were scaled from the prototypes [10] and are shown in Fig.2.

Cook's original perforated wall [13] (seen in Fig. 2 of reference 19) was found to induce faster mixing of the shear layer springing from the top edge. An alternative approach used in this study was to increase the periphery by 'folding' the top edge into castellations, resulting in the walls shown in Fig. 3 (WALL T1 and WALL T2) of 133-mm and 167-mm mean heights. The taller wall was also raised to a mean height of 267 mm (WALL T2 + 100 mm) by placing it on top of the wall shown in Fig. 1 (100 mm WALL). The inspiration for this toothed form of wall was not unconnected with the success of the Standen spires [12]. A version of Counihan's [10] wall (CASTELLATED WALL), 58 mm high to the base of the castellations, was scaled in proportion to match the 400-mm-high vorticity generators. Three types of surface roughness were used. The layer of 14 mm gravel shown in Fig. 4 was spread on the working-section floor. An excellent consistency of cover was obtained by using a 300-mm wide plastic dust-pan as a spreading device. (With the aid of a brush, the dust-pan also proved very useful for removing the gravel after tests!) Hardwood blocks, 100 mm × 50 mm × 50 mm (BLOCKS), were placed by hand in the diamond array shown in Fig. 1 to give an area density of 15%. The third form of roughness was the same as that previously used at Bristol by Cook [13], formed by glueing inverted plastic coffee-dispenser cups onto hardboard panels in a diamond array at an area density of 11% (CUPS). The diamond array was adopted in preference to the rectangular array of Counihan [11] as it was felt that each element would be in the faster air from between the elements of the preceding row and thus have a greater drag. The consequences of this choice will be discussed later.

Measurements were made of mean velocity and all three turbulence components. The velocity signals were acquired by conventional X-probe hot-wire anemometry, using the DISA 55P51 probe shown in Fig. 4. The velocity signals were monitored as Lissajous' figures on a storage oscilloscope, so that for each measurement a picture was built up of the extreme excursions of the velocity vector in the measurement planes uv and uw. This technique was demonstrated by Cook et al. [20] to be a useful method of detecting if the extreme excursions exceeded the resolution range ($\approx \pm 40°$) of the probe in the high-intensity turbulence close to the ground. At no time were the extreme excursions clipped to the extent indicated in Fig. 10c of

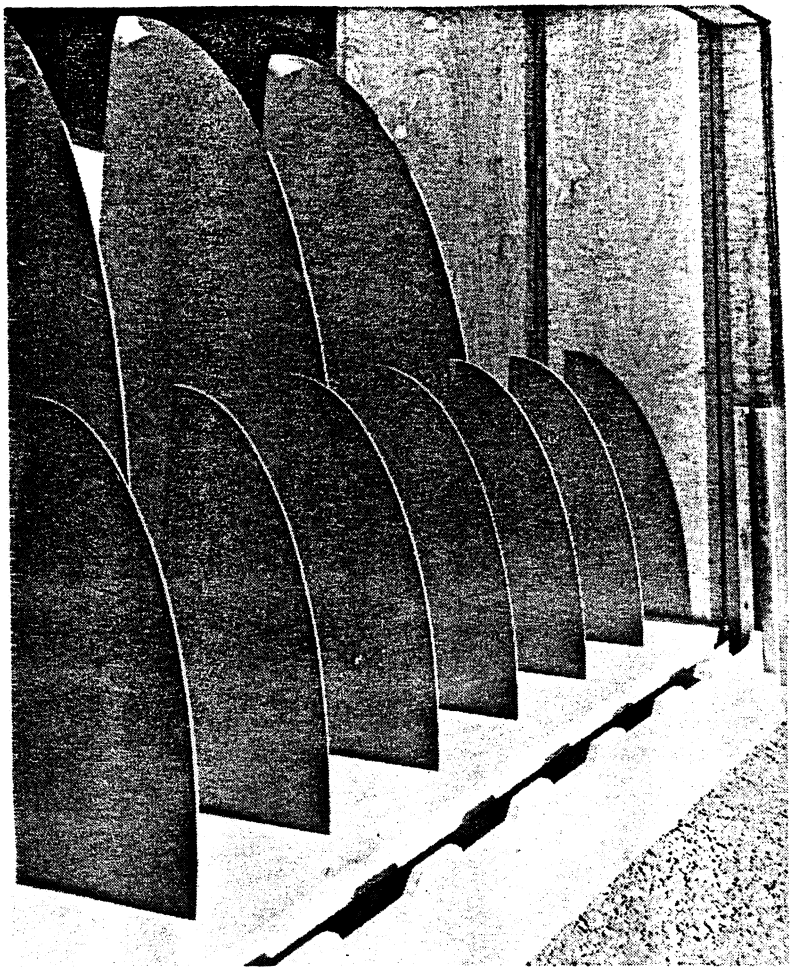

Fig. 2. Counihan-type elliptic wedge vorticity generators and castellated wall.

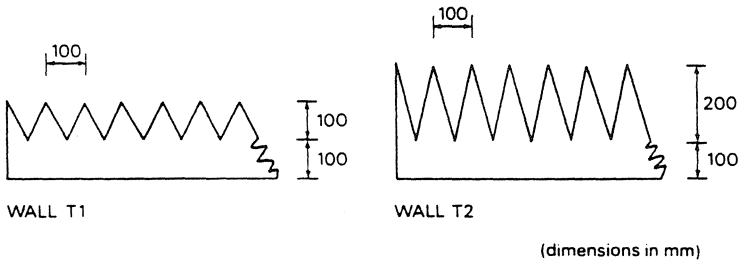

Fig. 3. The toothed walls.

reference 20. For measurements over the GRAVEL and CUPS roughnesses, the probe was traversed using the vertical motion of the three-component rig in the test area. The 450-mm maximum vertical travel of the rig proved inadequate for the deeper boundary layers. A simpler single-component rig, able to traverse the full 1-m height of the tunnel, was used for the BLOCKS roughness.

Analysis was performed in real-time by a digital data processor on-line to the wind tunnel. Values of the mean velocity U, the u, v and w r.m.s. intensities and the $-uw$ Reynolds stress were computed at each measurement position, then stored on magnetic disc. Measurements of power spectral density were made at selected heights over the frequency range 0.1 Hz—1 kHz using the FFT method [21]. The conflicting requirements of frequency range and discretion were resolved by analysing to 10 Hz, 100 Hz and 1 kHz sequentially, then forming a composite spectrum.

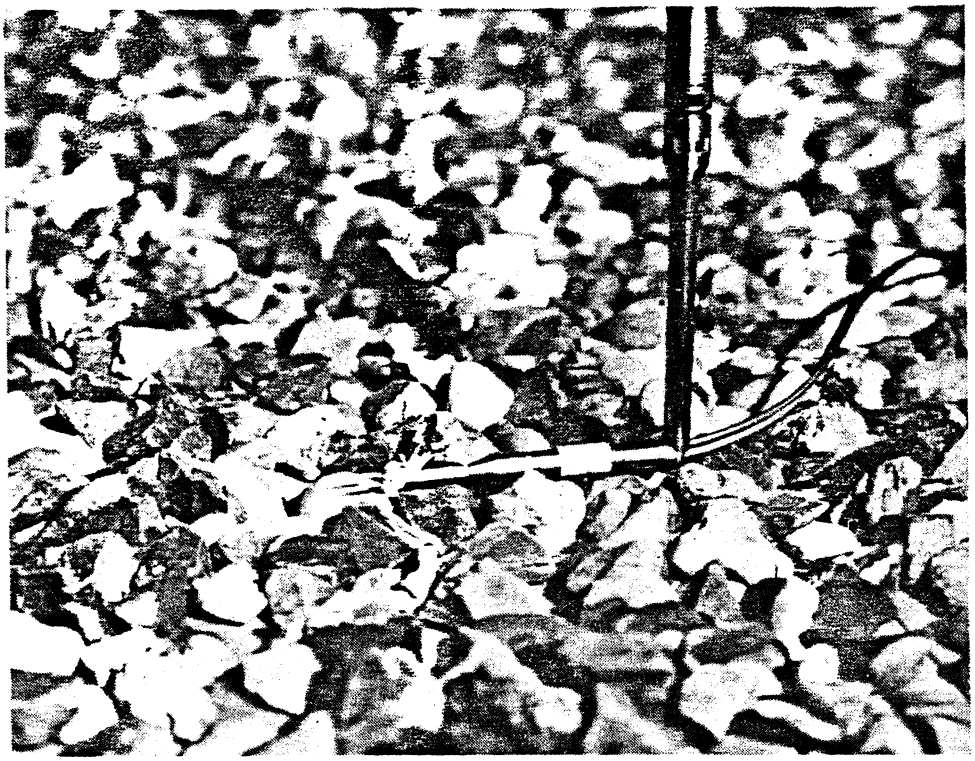

Fig. 4. Hot-wire *X*-probe over 14-mm GRAVEL roughness.

4. Prototype atmospheric wind data

The selection of prototype atmospheric data was discussed recently by Cook [22], when describing a process for determining the model scale factor. The scaling process was adopted for this work and the same atmospheric data set by ESDU [3,4] was used.

5. Results

(a) Mean velocity profiles

The discussion by Cook [22] on procedures for fitting the measured mean velocity profile near the ground surface to the logarithmic law-of-the-wall

$$\frac{U}{u_*} = \frac{1}{k}\ln\left(\frac{z-d}{z_0}\right)$$

was made on the basis of the measurements over the GRAVEL roughness presented in Fig. 5. It was concluded that the use of a measured Reynolds stress $-uw$ to determine a value for u_* gave more consistent results than the conventional 'error-in-origin' method [23] as the number of unknowns was reduced from three to two. The modified fitting procedure was described as a 'fit-to-known-slope'. A fit-by-eye was adopted in preference to a least-mean-squares method as advocated by Stearns [24] since the latter requires prior knowledge of the height range in which the law-of-the-wall is valid. Inclusion of data points in the upper 'velocity-defect-law' layer, or points close to the surface which may be influenced by a single roughness element, into the least-mean-squares procedure produces a poor fit. When a preliminary fit-by-eye was performed to determine the range of validity on a number of profiles, the results were considered to be sufficiently good not to warrant the more complex process. The high packing density of the GRAVEL surface ensured that the surface shear stress was spatially uniform, resulting in smooth profiles of Reynolds stress which showed a clear, flat

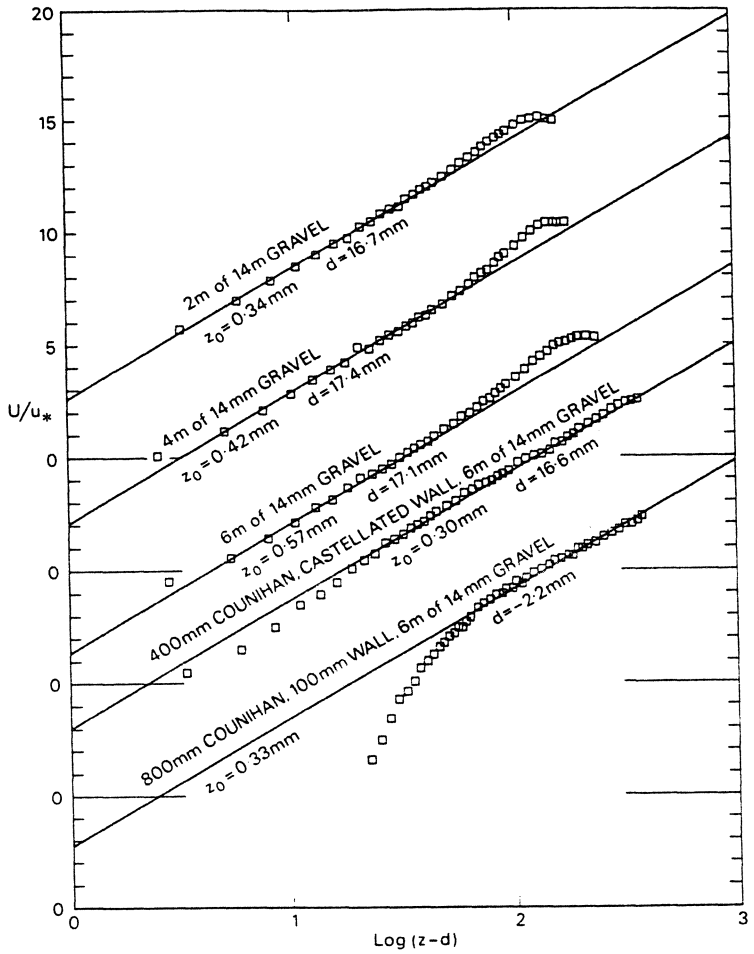

Fig. 5. Mean velocity profiles for a family of 'rural' simulations.

maximum just above the surface. As a contrast, the BLOCKS and CUPS roughness elements acted as individual momentum sinks, producing spatially non-uniform distributions of Reynolds stress near the surface. The mean velocity profiles over the BLOCKS roughness presented in Fig. 6 were obtained by traversing on the centre-line of the nearest upstream element at the centroid of the triangle formed by that element and the two nearest downstream elements. The measured profiles of Reynolds stress, presented later, showed two maxima; the one highest from the ground was taken to represent the overall shear stress and was used to determine u_*, while the one closest to the ground was taken as due to the individual effect of the upstream element.

The boundary layers of Fig. 5 deepened as the fetch of GRAVEL was increased, displaying the characteristic parabolic deviation in the velocity-defect-law layer above the logarithmic law. The same effect was produced in both Figs. 5 and 6 by increasing the height of the barriers. In the case of the BLOCKS roughness, the boundary layers eventually reached the wind-tunnel roof. When the barrier height was large with respect to the roughness, two anomalies became apparent; a deepening region near the surface no longer fitted the logarithmic law and the indicated zero-plane displacement d reduced, eventually becoming negative. The fact that the flow 'lost touch' with the physical surface indicates that a length scale other than the aerodynamic roughness length was controlling the flow, namely a length scale from the barrier. If so, the lower region should fit to the logarithmic law as before, as an internal wall layer. Figure 7 illustrates the fit obtained to the lower region for the highest barrier GRAVEL and BLOCKS cases, when the zero-plane displacement returns positive but the profile diverges uncharacteristically *below* the logarithmic-law line. Also included in Fig. 7 is a profile obtained when two roughness-length scales were deliberately represented

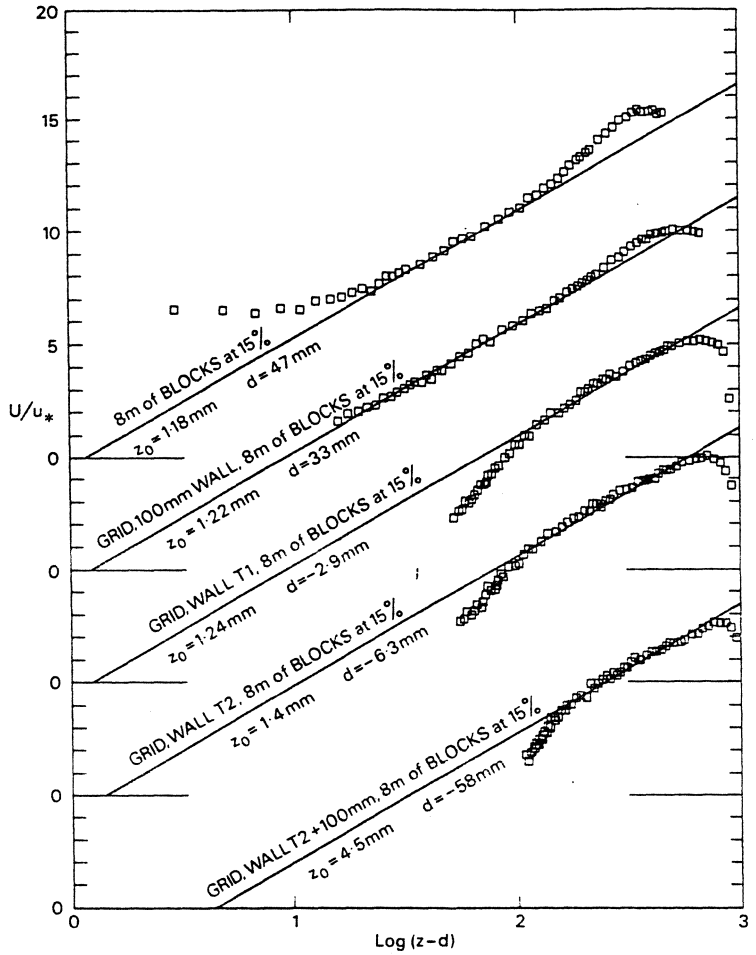

Fig. 6. Mean velocity profiles for a family of 'urban' simulations.

simultaneously by mixing a 6-m fetch of GRAVEL surface with 50-mm walls at 2-m spacings* and fitting the logarithmic law to the lower (GRAVEL) layer. The upper layer is seen to diverge below the logarithmic-law line before returning above to form the velocity-defect-law region. Fitting this upper layer to the logarithmic law again produces a negative value for d. It is suggested that the three profiles of Fig. 7 are produced by the same double-length-scale process, that the GRAVEL profile continued to form a velocity-defect-law region above the traverse limit and that this was prevented in the BLOCKS profile by the boundary layer reaching the tunnel roof.

The variation of the law-of-the-wall length parameters z_0, the aerodynamic roughness length, and d, the zero-plane displacement, with the mean wall height is summarised for (a) the BLOCKS and (b) the CUPS roughnesses in Fig. 8 based on a fit to the deeper upper layer. Also included in Fig. 8b are values for a roughness fetch of 4 m (solid symbols) from Cook [13]. While the barrier remains low, z_0 and d remain sensibly constant, but once the barrier starts to affect the flow, the effect (a change in value with increasing height) is rapid. The effect is also fetch-dependent, especially as the roughness within the increasingly long separation bubble behind the wall must have a reduced effect on the flow, although the three fetches illustrated in Fig. 8 are hardly sufficient to quantify the effect satisfactorily.

*These data come from a study of a 'two roughness-length scale problem' which is relevant to the simulation of typical British farmland terrain, i.e. fields alternating with wooded hedgerows, and which may be reported at a later date.

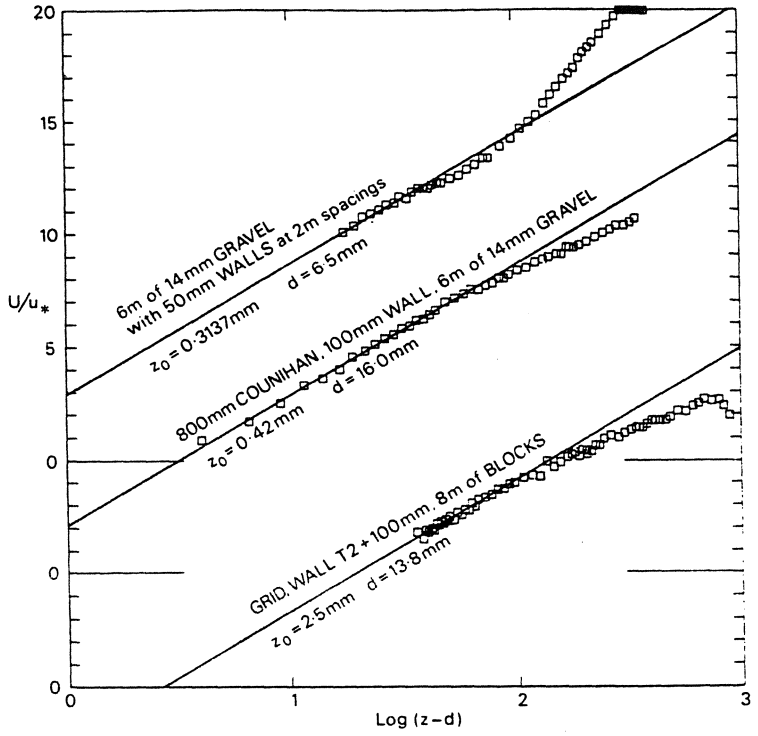

Fig. 7. Mean velocity profiles with surface region fitted to logarithmic law.

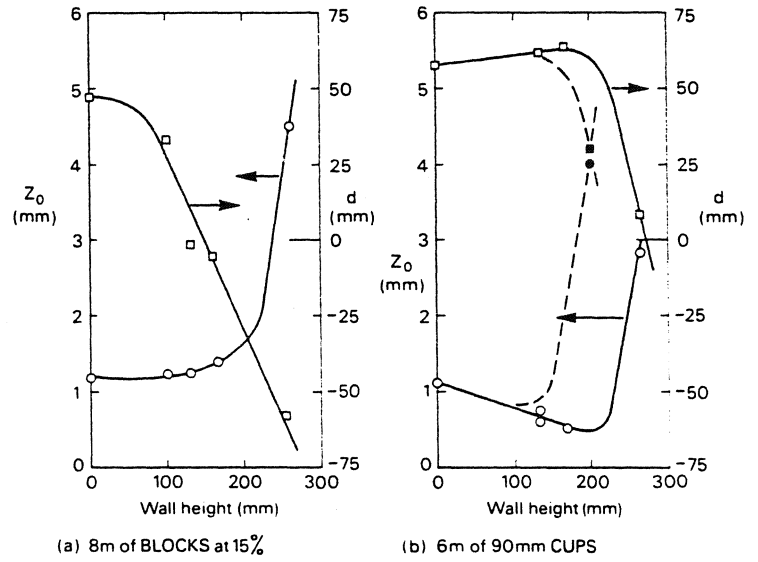

Fig. 8. Law-of-the-wall parameters z_0 and d.

The relative effectiveness of the BLOCKS and CUPS roughness can also be assessed from Fig. 8. Despite their height, the high aspect ratio CUPS give only about half the aerodynamic roughness length of the BLOCKS. The choice of a diamond grid pattern had the opposite of the intended effect. Placing each successive row of elements in the faster air between the elements of the preceding row encourages the air to flow *over* rather than around the elements, increasing the zero-plane displacement. Comparison with Counihan's results with a rectangular array [16] shows the BLOCKS to be only one-fifth as rough and to give double the zero-plane displacement.

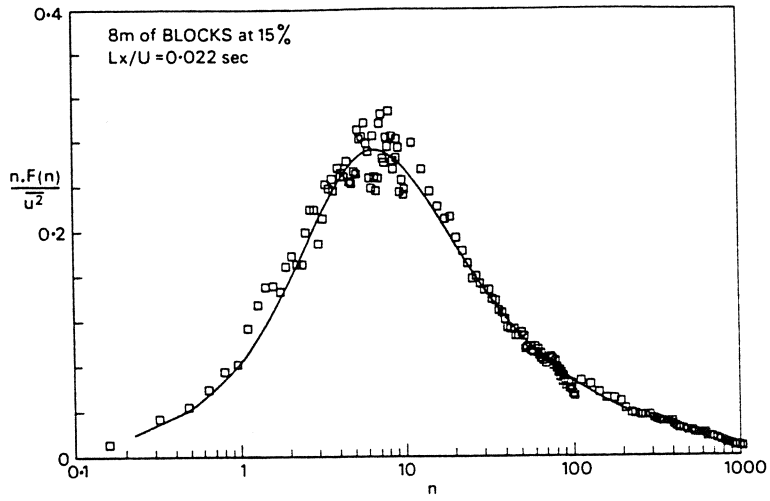

Fig. 9. Spectrum of streamwise turbulence at z = 300 mm with no barrier.

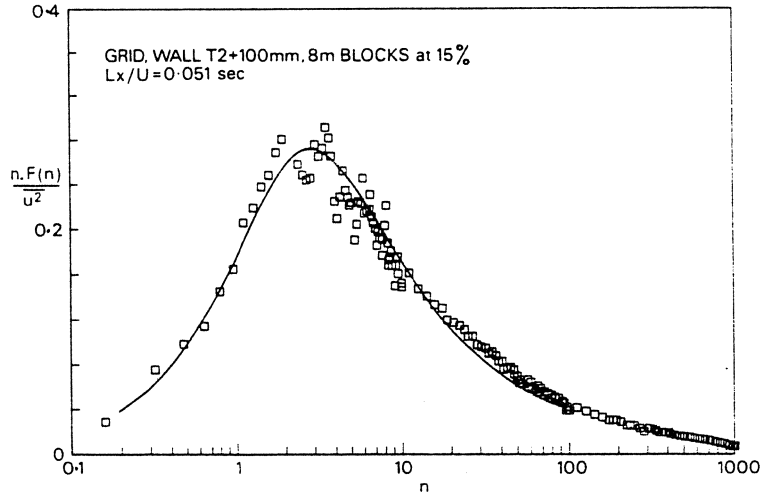

Fig. 10. Spectrum of streamwise turbulence at z = 300 mm with highest barrier.

(b) Streamwise turbulence spectra and integral lengths

The spectra presented as Figs. 9 and 10 were measured at a height of 300 mm after an 8-m fetch of BLOCKS and represent the extremes of no barrier and highest barrier respectively. The solid line is the ESDU [4] atmospheric spectrum fitted to the measured results to give the values of Lx/U marked on the figures. The model results fitted the shape of the prototype curve to the same degree in every case.

Presented in Fig. 11 are the values of integral length Lx derived by this procedure for the BLOCKS and CUPS cases corresponding to the law-of-the-wall data in Fig. 8. The measured values increase with the mean wall height until the boundary layer fills the wind tunnel, after which there is no further increase. Indeed, a slight reduction in value is indicated with the highest wall. The solid symbol in Fig. 11b again indicates the value obtained by Cook [13] with a 4-m fetch, and shows that Lx is less fetch-dependent than the parameters z_0 and d. In Fig. 11a, the values for z = 450 mm with no barrier and with the 100-mm WALL are low because the boundary layers were sufficiently shallow for the measurement point to be in the velocity-defect-law region.

(c) Profiles of turbulence intensity and Reynolds stress

Profiles of turbulence intensity and Reynolds stress after 8 m of the BLOCKS roughness are presented as Figs. 12—16 inclusive, corresponding to the mean velocity profiles of Fig. 6, in order of increasing barrier height.

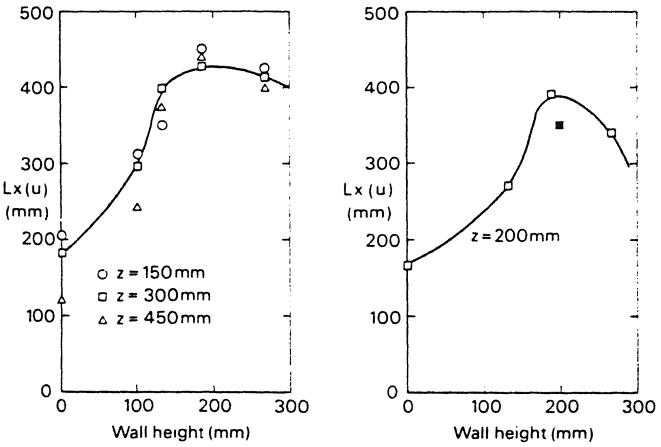

Fig. 11. Longitudinal integral length parameter of streamwise turbulence.

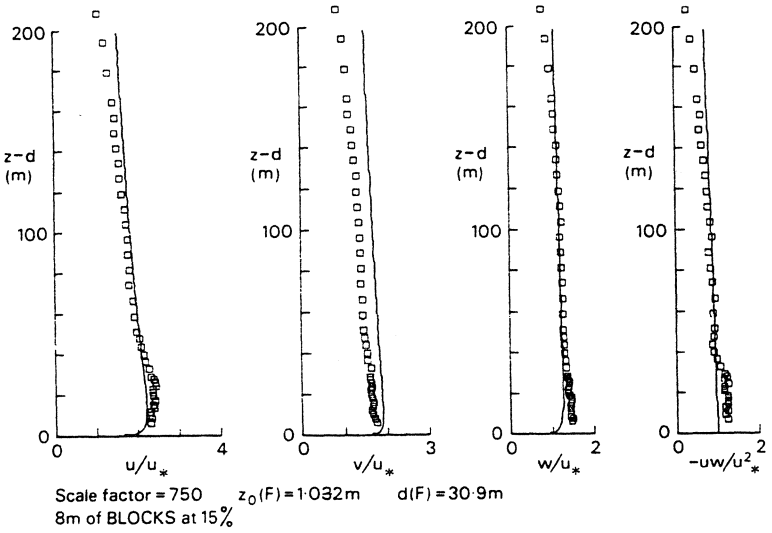

Fig. 12. Turbulence profiles.

The scaling process [22] has been implemented; thus the resulting scale factor, full-scale values of z_0 and of d are given and the vertical scale is in metres full-scale in each case. The prototype atmospheric profiles from the ESDU [4] data have been superimposed as the solid lines. Most of the profiles show the effect of the nearest upstream roughness element as a local maximum at the bottom of each profile. The data for the naturally grown layer (Fig. 12) show an excellent fit to the prototype data, except that the cross-stream intensity v is a little low. In all the cases with a barrier except for the highest barrier, Figs. 13, 14 and 15, the vertical intensity w matches the prototype data well, but the other profiles decay too rapidly with increasing height. With the highest barrier (Fig. 16), the profiles tend not to decay rapidly enough and the vertical intensity w actually increases with height. There would therefore appear to be an optimal barrier height, between the two highest, for which an excellent fit to the prototype data should again be obtained.

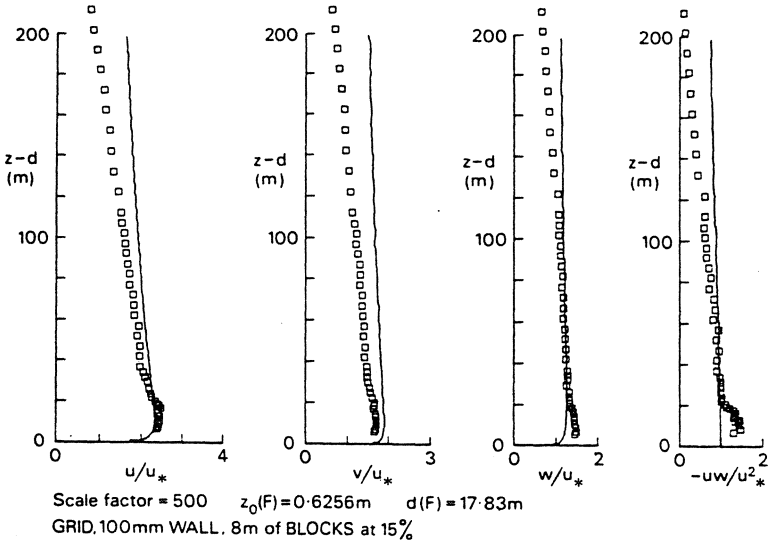

Scale factor = 500 $z_0(F) = 0{\cdot}6256$m d(F) = 17·83m
GRID, 100mm WALL, 8m of BLOCKS at 15%

Fig. 13. Turbulence profiles.

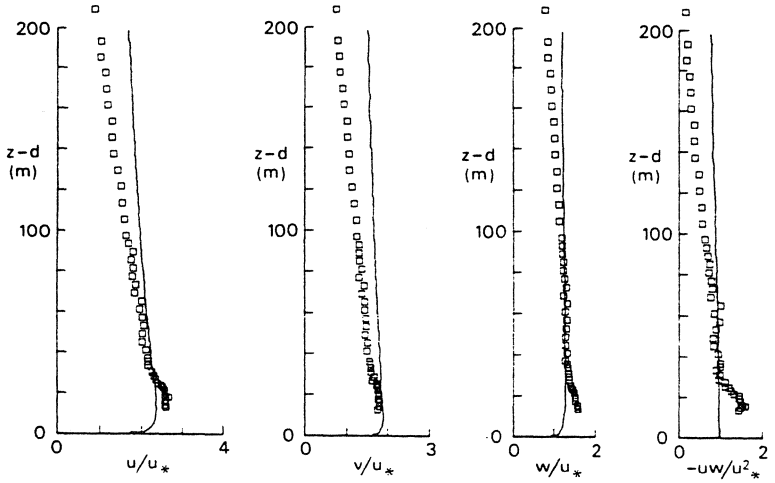

Scale factor = 400 $z_0(F) = 0{\cdot}4878$m d(F) = 6·494m
GRID, WALL T1, 8m of BLOCKS at 15%

Fig. 14. Turbulence profiles.

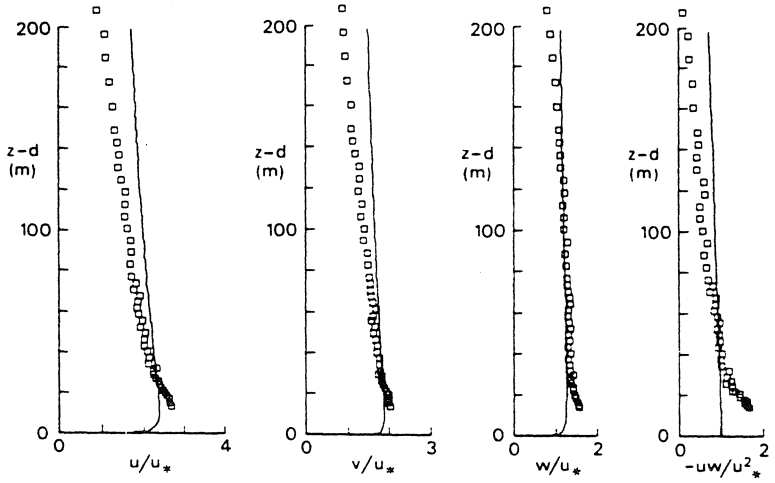

Scale factor = 300 z(F) = 0·3673m d(F) = 1·381m
GRID, WALL T2, 8m of BLOCKS at 15%

Fig. 15. Turbulence profiles.

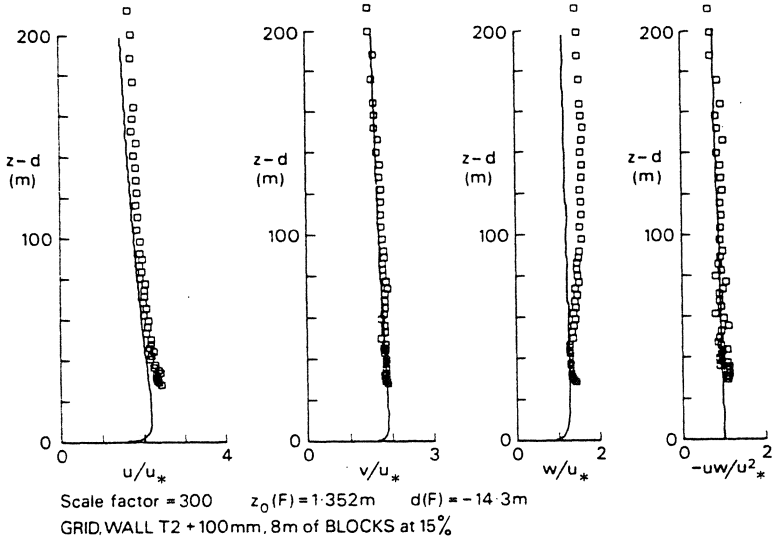

Fig. 16. Turbulence profiles.

6. Comments and conclusions

An unpublished survey of the area density of buildings by the Building Research Station has revealed that, for 732 dwellings in locations throughout Britain, the mean density was 15% within a 50-m radius and 10% within a 150-m radius. In a similar survey of 110 housing schemes reported by Turner [25], the mean density was also 15%, more than half the schemes being in the range 10—20%. The densities of the BLOCKS and CUPS roughnesses were therefore typical of actual conditions. The flaw in the original logic of selecting a diamond array is obvious in retrospect. In frontal projection, the BLOCKS roughness presented 78% solidity to the flow, whereas a rectangular type array of the same 15% area density would have presented only 39% solidity. The use of a standard height element, rather than a range of heights as used by Davenport and Isyumov (Fig. 1 of reference [1]), may have been another contributory factor as Perry et al. [26] found the skimming type of flow to be sensitive to variation in element height. A recent study by Edwards [27] has revealed a previously unreported cyclic flow pattern in diamond arrays of roughness elements at small transverse pitches. The 'horseshoe vortices' at the wake edges of elements in odd-numbered rows impinged on the elements in the even-numbered rows. This applied vorticity was equal, but of opposite sign, to the horseshoe vortices that should have formed on the elements of the even rows and they were effectively cancelled out, leaving a small closed separation bubble behind each element instead of a wake. Edwards originally noted the effect when measuring drag and heat-transfer coefficient of a small number of rows, when the odd-numbered rows consistently gave high values and the even-numbered rows gave low values. Subsequent tests showed that the effect increased in strength and stabilised over longer fetches. A simple test for the occurrence of this phenomenon is the pigment-streak flow-visualisation technique. The test proved negative when applied to the roughness arrays used in this study, revealing no differences in the wake structure behind both odd- and even-numbered rows as illustrated by Fig. 17.

The BLOCKS roughness produced values of equivalent full-scale aerodynamic roughness parameter z_0 of 1 m at 1/750 (when the element height scaled to 38 m) which is typical of British city-centre conditions, and values of z_0 from 0.3 to 0.5 m at between 1/300 and 1/400 (when the element height scaled between 15 m and 20 m) which is typical of suburban conditions. The equivalent full-scale heights of the elements were only a little larger than typical building heights for the terrain type. Only in the few cases of 'planned' development is it possible for many along-wind street lines to exist, equivalent to the rectangular array, and then only for a few wind directions.

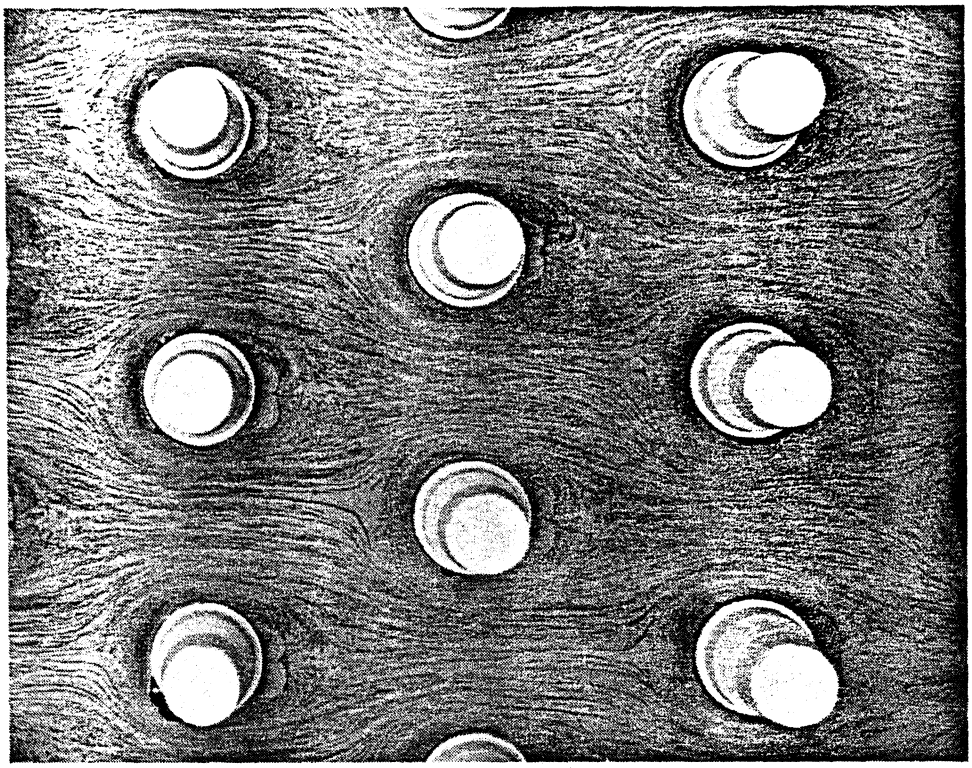

Fig. 17. Pigment-streak visualisation of surface flow through CUPS roughness.

Urban development is generally far less regular than either a diamond or rectangular array but, on the grounds discussed, the former is more typical.

The barrier had its intended effect of increasing the boundary-layer depth h and therefore Lx without significantly altering the law-of-the-wall parameters u_*, z_0 and d provided the mean height did not exceed twice the element height of the individual BLOCKS and CUPS elements and about five times the 'height' of the GRAVEL elements. Since a larger surface roughness tolerated a higher barrier, larger models (smaller scale factors) can be more readily achieved for urban simulations than for rural simulations. The transition from a 'full-depth' to a 'part-depth' simulation was the natural result of the boundary layer filling the height (1 m) of the wind tunnel, after which no further increase in Lx was obtained with barrier height. The profile of Lx decayed above half the tunnel height owing to the presence of the roof. If this is equated to the Lx profile in naturally grown boundary layers, where Lx decreases above 0.3 h by dilution of the turbulence through intermittency with the smooth flow [28], the maximum size of a part-depth simulation is for an equivalent boundary-layer height h of 1.7 times the height of the wind tunnel. Larger simulations can only be achieved if some of the modelling requirements are relaxed. For example, a largely 'artificial' rural simulation at 1/100 can be obtained by grading the surface roughness from large (180-mm high) elements upstream to small (14-mm GRAVEL) elements downstream if Lx is matched over the lower half of the wind tunnel only; in which case only the lower 50 m of the atmospheric boundary layer is represented.

In conclusion, it is evident from the data that entirely naturally grown boundary layers give the best simulations, but at large scale factors. Smaller scale factors require that some artificial assistance be given, inevitably reducing the quality of the simulation. The degree of assistance and the degree of 'artificiality' of the resultant simulation is a matter of choice, and this paper goes some way towards quantifying the effects.

Nomenclature

d zero-plane displacement in logarithmic law-of-the-wall
F power spectral density function
k Von Karman constant = 0.40
Lx longitudinal integral length parameter for streamwise turbulence component
n frequency
U mean velocity
u_* friction velocity in logarithmic law-of-the-wall
u r.m.s. intensity of streamwise turbulence component
v r.m.s. intensity of cross-wind turbulence component
w r.m.s. intensity of vertical turbulence component
$-uw$ Reynolds stress (negative covariance of streamwise and vertical turbulence components)
z height above ground surface
z_0 aerodynamic roughness length in logarithmic law-of-the-wall

In Figs. 14—18, (F) indicates equivalent full-scale values.

REFERENCES

1 A.G. Davenport and N. Isyumov, The application of the boundary layer wind tunnel to the prediction of wind loading, Wind Effects on Buildings and Structures, Ottawa, Canada, September 1967, University of Toronto Press, pp. 210—230.
2 J.E. Cermak and S.P.S. Arya, Problems of atmospheric shear flow and their laboratory simulation, Boundary-Layer Meteorol., 1(1970) 40—60.
3 Characteristics of windspeed in the lower layers of the atmosphere near the ground: strong winds (neutral atmosphere), ESDU Data Item No. 72026, Engineering Sciences Data Unit, London, 1972.
4 Characteristics of atmospheric turbulence near the ground, ESDU Data Items Nos. 74030, 74031, 75001, Engineering Sciences Data Unit, London, 1974, 1975.
5 J. Counihan, Adiabatic atmospheric boundary layers: a review and analysis of data from the period 1880—1972, Atmos. Environ., 9(1975) 871—905.
6 D.M. Deaves and R.I. Harris, A mathematical model of the structure of strong winds, CIRIA Report No. 76, 1978.
7 J.C.R. Hunt and H. Fernholz, Wind tunnel simulation of the atmospheric boundary layer: a report on Euromech 50, J. Fluid. Mech., 70(1975) 543—559.
8 P.R. Owen and H.K. Zienciewicz, Production of uniform shear flow in a wind tunnel, J. Fluid Mech., 2 (1957).
9 J.W. Elder, Steady flow through non-uniform gauzes, J. Fluid Mech., 5 (1959).
10 J. Counihan, An improved method of simulating an atmospheric boundary layer in a wind tunnel, Atmos. Environ., 3 (1969) 197—214.
11 J. Counihan, Simulation of an adiabatic urban boundary layer in a wind tunnel, Atmos. Environ., 7(1973) 673—689.
12 N.M. Standen, A spire array for generating thick turbulent shear layers for natural wind simulation in wind tunnels, Laboratory Technical Report LA-94, National Aeronautical Establishment, Ottawa, Canada, May 1972.
13 N.J. Cook, On simulating the lower third of the urban adiabatic boundary layer in a wind tunnel, Atmos. Environ., 7(1973) 691—705.
14 J. Armitt and J. Counihan, The simulation of the atmospheric boundary layer in a wind tunnel, Atmos. Environ., 2(1968) 49—71.
15 J. Counihan, Further measurements in a simulated boundary layer, Atmos. Environ., 4(1970) 259—275.
16 J. Counihan, Wind tunnel determination of the roughness length as a function of the fetch and the roughness density of three-dimensional roughness elements, Atmos. Environ., 5(1971) 637—642.
17 H.M. Nagib, M.V. Morkovin, J.T. Yung and J. Tan-Atichat, On modelling of atmospheric surface layers by the counter-jet technique, AIAA Paper No. 74-638, AIAA 8th Aerodyn. Testing Conf., Bethesda Maryland, U.S.A., July 1974.
18 R.V. Barrett, A versatile compact wind tunnel for industrial aerodynamics, Atmos. Environ., 6(1972) 491—498.
19 N.J. Cook, A boundary layer wind tunnel for building aerodynamics, J. Ind. Aerodynam., 1(1975) 3—12.
20 N.J. Cook, B.H. Coulson and W. McKay, Wind conditions around the Rock of Gibraltar, J. Ind. Aerodynam., 2(1978) 289—309.
21 J.S. Bendat and A.G. Piersol, Random Data: Analysis And Measurement Procedures, Wiley, New York, 1971, pp. 322—336.

22 N.J. Cook, Determination of the model scale factor in wind-tunnel simulations of the adiabatic atmospheric boundary layer, J. Ind. Aerodynam., 2(1978) 311—321.
23 R.A. Antonia and R.E. Luxton, The response of a turbulent boundary layer to a step change in surface roughness. Part 1. Smooth to rough, J. Fluid Mech., 48(1971) 721—761.
24 C.R. Stearns, Determining surface roughness and displacement height, Boundary-Layer Meteorol., 1(1970) 102—111.
25 J. Turner, A comparative study of the land use and built form of 110 schemes, Technical Study No. 31, The Architects' J., 158 (1973) 265—280.
26 A.E. Perry, W.H. Schofield and P.N. Joubert, Rough wall turbulent boundary layers, J. Fluid Mech., 37(1969) 383—413.
27 F.J. Edwards, Some interference effects in flows around surface protrusions, Paper 8, 52nd. Industrial Fluid Mechanics Research Meeting, NPL Teddington, 12th. Jan. 1977.
28 R.A. Antonia and R.E. Luxton, The response of a turbulent boundary layer to an upstanding step change in surface roughness, Trans. ASME, J. Basic Eng., 93(1971) 22—32.

Journal of Industrial Aerodynamics, 2 (1977/1978) 311—321

DETERMINATION OF THE MODEL SCALE FACTOR IN WIND-TUNNEL SIMULATIONS OF THE ADIABATIC ATMOSPHERIC BOUNDARY LAYER*

N.J. COOK

Department of the Environment, Building Research Station, Garston, Watford (U.K.)

(Received March 6, 1977)

Summary

A process is proposed for determining the model scale factor in contemporary full-depth or part-depth simulations of the atmospheric boundary layer in a wind tunnel.

1. Introduction

In order to simulate the effects of wind on buildings and structures at model scale, the properties of the atmospheric boundary layer must be linearly scaled by the same scale factor as the building model. When simulation techniques gave only simple representation of a few of the boundary-layer characteristics, mean velocity profile for example, scaling was not a great problem. Contemporary simulation techniques attempt to represent much more detail, and include the fluctuating velocity components of atmospheric turbulence. Recent extensive reviews of full-scale wind data [1—3] present the characteristics of the prototype atmospheric wind on a parametric basis. There are now many parameters to be considered in the scaling process and, in order to ensure consistency of result, it is necessary to adopt a standard approach to the problem. It is suggested that two key properties of the flow can be defined, expressed as lengths, which are sufficient to determine an initial scale factor for a proposed model and that the other flow properties should then be checked against the full-scale prototype at this scale factor.

2. Prototype atmospheric wind data

The task of deriving prototype atmospheric wind data is particularly daunting and it is fortunate that the two recent reviews, by ESDU [1,2] and by Counihan [3], are available. The ESDU data have been collated and only the final design data are presented graphically in a parametric form. On the other hand, Counihan presents and discusses the experimental data, pointing out conflicts but leaving the final decisions to the reader. The choice of the data source does not affect the philosophy of the scaling approach and the ESDU data are used for the sake of convenience.

Design curves for the mean velocity profile, for the turbulence component intensities, spectra and longitudinal integral lengths and also for the Reynolds stress are presented as Figs. 1—4. In these figures, the length dimension has been retained, but velocities have been normalised against U_{10}, the mean velocity at the meteorological standard height of 10 m. In the design spectra, the frequency ordinate nL_x/U has been made non-dimensional using the local mean velocity and relevant longitudinal integral length. It should be noted that none of the design curves extends above a height of 200 m, beyond

*Crown Copyright 1977 — Building Research Establishment, Department of the Environment.

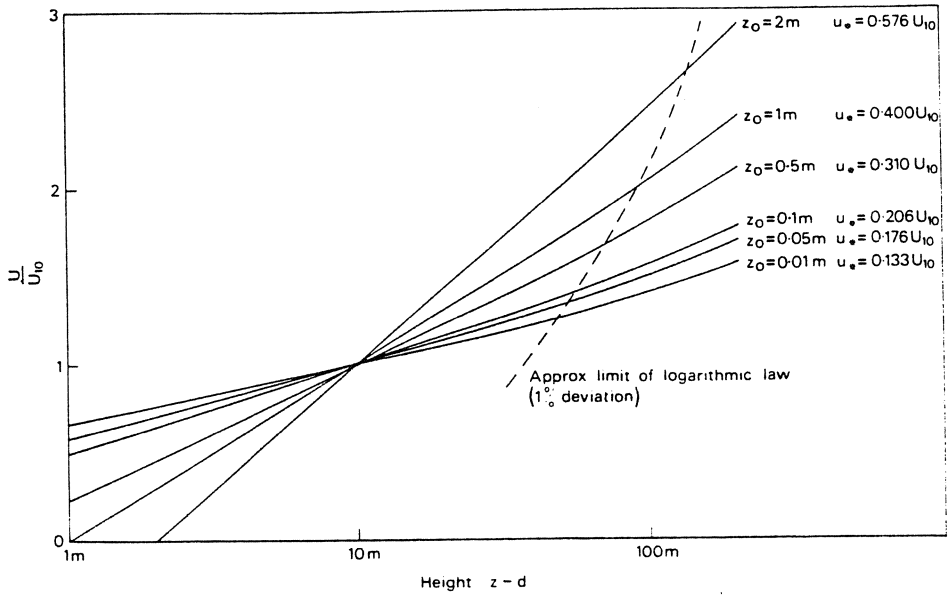

Fig. 1. Design mean velocity.

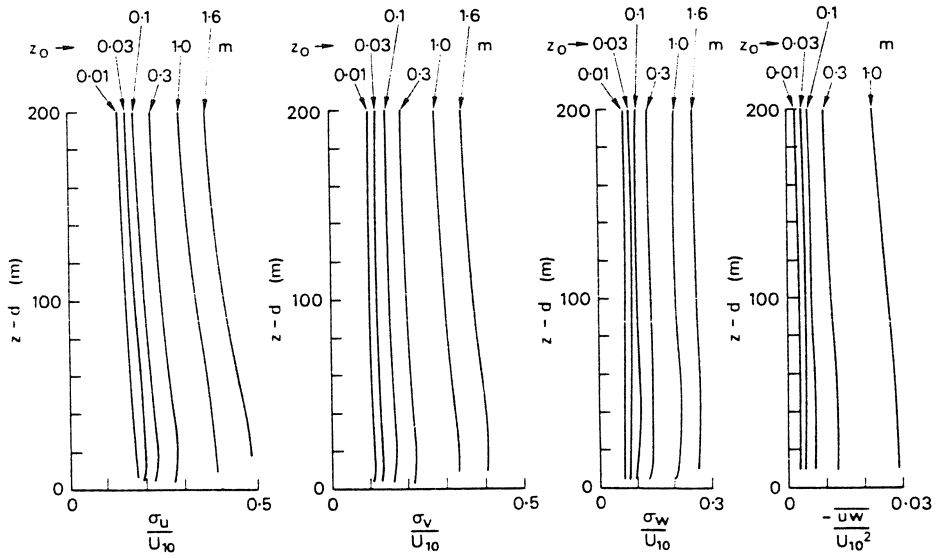

Fig. 2. Design turbulence intensities and Reynolds stress.

which there are insufficient full-scale data. Two parameters specifically omitted from the design curves are the boundary-layer height, as it is often not physically realisable when model scales are attempted at which the boundary layer height would exceed that of the wind tunnel (the 'part-depth' simulation approach [4]), and the exponent α in thepower-law representation of the mean velocity profile, because this parameter is scale-independent. Moreover, since the buildings occupy a small fraction of the boundary-layer height, these parameters are not as important as those descriptive of the flow near the ground surface.

The two key parameters should, together, describe the mean velocity and the turbulence characteristics over the depth of the simulation that is required, so as to be applicable to both full-depth and part-depth simulation approaches. They must both have the dimension of length and be related in such a way that any combination of values results in a unique value of scale factor. Accordingly, the first key parameter is the roughness length z_0 which is descriptive of the mean velocity profile and is a measure of the surface roughness, and the second key parameter is the longitudinal integral length of the u-component of turbulence L_{x_u}, which is a measure of the dominant eddy size in the turbulence. The roughness length z_0 has a unique value in any given boundary layer, but the integral length L_{x_u} is a function of height above ground.

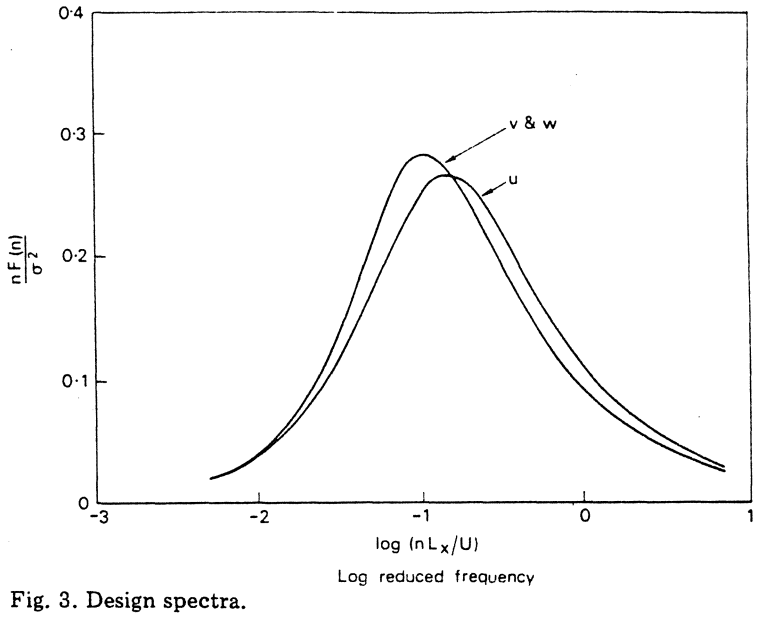

Fig. 3. Design spectra.

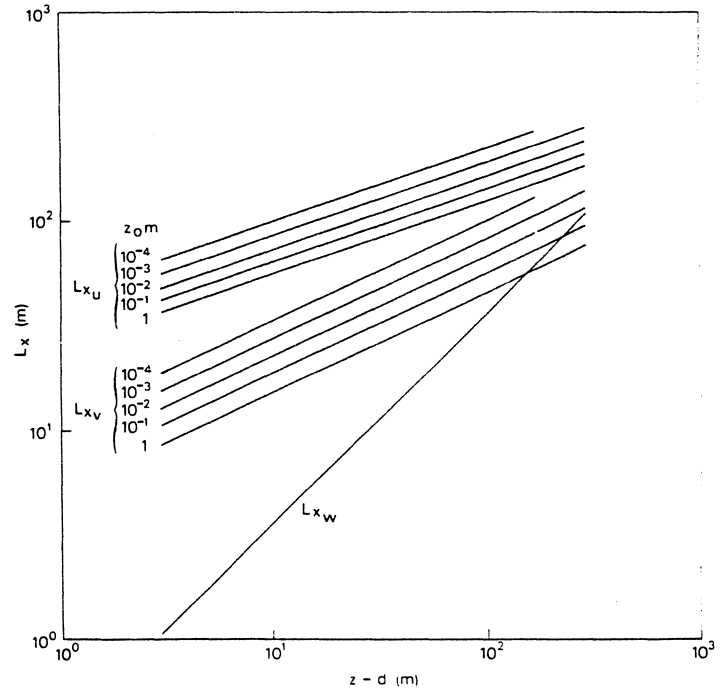

Fig. 4. Design integral length scales.

3. Determination of the key parameters

The roughness length parameter z_0 is determined by fitting the measured mean velocity profile near the ground surface to the logarithmic law-of-the-wall

$$U = \frac{u_*}{\kappa} \ln\left(\frac{z-d}{z_0}\right)$$

When the conventional 'error-in-origin' method [5] is used there are three unknowns, u_*, d and z_0, and the data are fitted for best straight line. If an independent estimate of the friction velocity u_* is obtained by surface shear-stress measurement, when $u_* = (\tau_0/\rho)^{\frac{1}{2}}$, or by measurement of the maximum Reynolds stress, when $u_* = (-\overline{uw})^{\frac{1}{2}}$, the unknowns are reduced to two. Values of friction velocity determined in a boundary layer over a gravel surface by the three methods are compared in Table 1.

TABLE 1

Comparison of friction-velocity estimates

u_*/U_{ref}	Mean value	Standard deviation
By error-in-origin method	0.083	0.022 (27%)
From surface shear stress	0.070	0.002 (3%)
From maximum Reynolds stress	0.071	0.004 (6%)

It is seen that the direct measurements give closely comparable results and much smaller variation than the error-in-origin method. This leads in turn to smaller variability in the roughness length estimates by the fitting procedure to the two unknowns d and z_0, which is now essentially a 'fit-to-known-slope'. Typical results for a full-depth and a part-depth simulation are shown in Figs. 5 and 6 respectively.

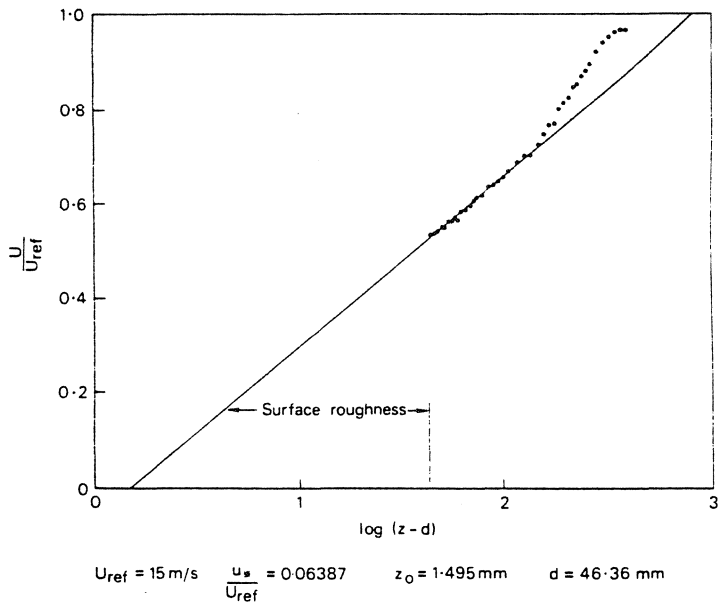

Fig. 5. Law-of-the-wall fit to mean velocity profile in typical full-depth simulation.

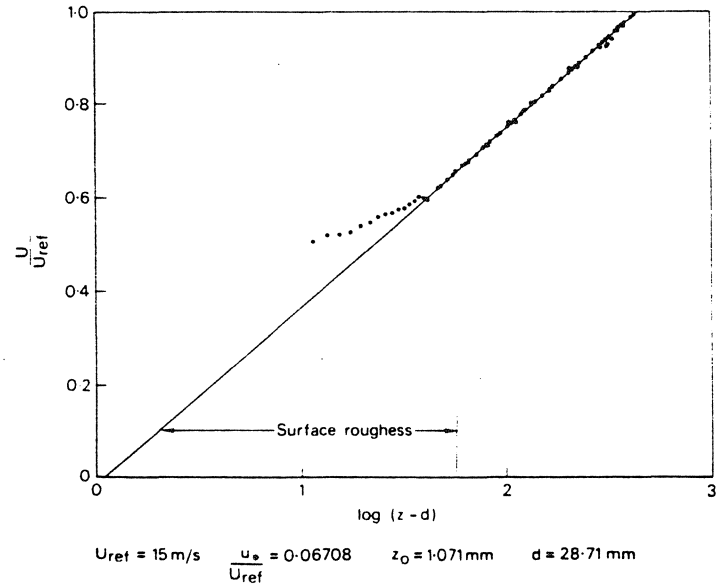

Fig. 6. Law-of-the-wall fit to mean velocity profile in typical part-depth simulation.

The longitudinal integral length L_{x_u} should be determined from true space-correlation measurements. However, owing to the practical difficulties of these two-point measurements in full scale, most atmospheric data are determined from auto-correlation or spectral measurements, when $L_{x_u} = U\int_0^\infty \rho_u\{t\}dt$ or $L_{x_u} = (U/4\sigma_u^2)F_u\ \{n = 0\}$ respectively, assuming that Taylor's hypothesis is valid. The value of L_{x_u} so obtained is effectively based on a single spectral estimate, that at the lowest measured frequency (nominally zero), and is subject to the same variability as that estimate. A more reliable result is obtained when the atmospheric data are fitted to the design curve for the u-component spectrum of Fig. 3 over the full frequency range measured, and this method is frequently used. When applied to the model spectrum, the method allows a certain amount of flexibility. In the event of the spectrum not matching the prototype exactly in shape, the fit may be biased to a restricted frequency range of particular interest, e.g. around the scaled natural frequencies of the building to be modelled. The process is illustrated by Figs. 7 and 8 for two heights in the typical part-depth simulation. The values of frequency, n, which appear on the figures correspond to $nL_{x_u}/U = 1$ on the design curve. As U is known at each height from Fig. 6, estimates of L_{x_u} are obtained.

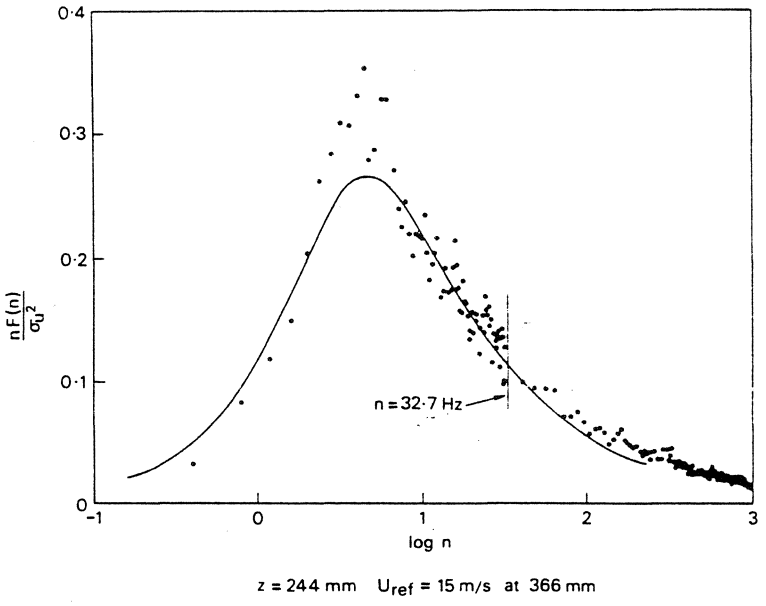

Fig. 7. u-component spectrum in typical part-depth simulation fitted to design curve.

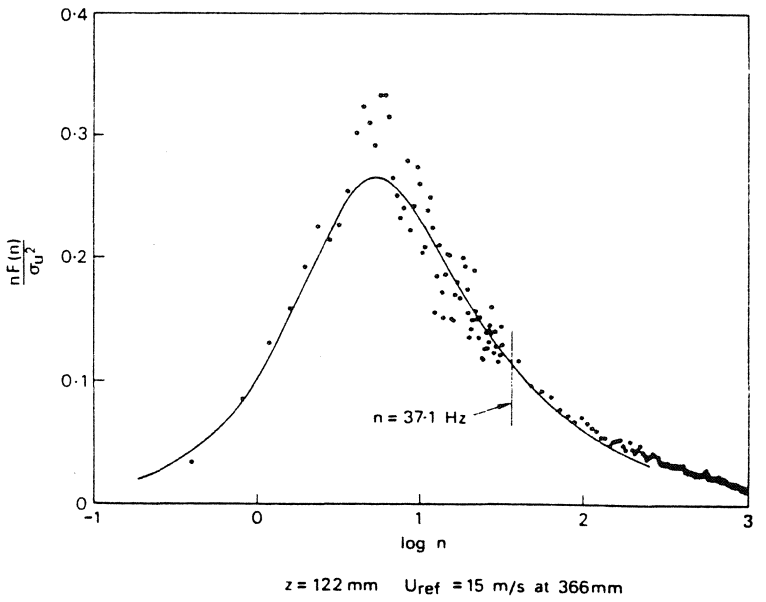

Fig. 8. u-component spectrum in typical part-depth simulation fitted to design curve.

4. The proposed scaling procedure

The first parameter z_0 is a constant, but the second parameter L_{x_u} has a functional dependence on the effective height $z - d$ and on z_0. The ESDU [2] data of Fig. 4 are fitted by the empirical equation

$$L_{x_u} = 25(z - d)^{0.35} z_0^{-0.063}$$

with all lengths expressed in metres. The scaling procedure makes use of this dependence.

The model scale factor S is determined by one of two methods:

(a) by graphical iteration on Fig. 4 or any other source of data for L_{x_u}.

(b) deterministically, using the empirical equation for L_{x_u}.

These methods are now demonstrated for the typical part-depth simulation at the height $z_M = 0.244$ m. (Subscript M denotes model values.) Here, $z_{0_M} = 0.00107$ m and $d_M = 0.0287$ m from Fig. 6. Also $n_M = 32.7$ Hz and $U_M = 13.2$ m/s at $nL_{x_u}/U = 1$ from Fig. 8, giving $L_{x_{u_M}} = 403$ mm.

(a) Graphical iteration

First iteration: an initial scale factor of $S_0 = 200$ is assumed and equivalent full-scale values (subscript F) for the roughness length and the effective height of the measurement are obtained. Thus:

$$z_{0_F} = S_0 z_{0_M} = 200 \times 0.00107 = 0.214 \text{ m}$$

$$(z - d)_F = S_0(z - d)_M = 200 \times 0.215 = 43.0 \text{ m}$$

and from Fig. 4 $L_{x_{u_F}} = 103$ m. The first iteration estimate of scale factor is

$$S_1 = L_{x_{u_F}}/L_{x_{u_M}} = 103/0.403 = 256.$$

Second iteration: The process is repeated using $S_1 = 256$. This time:

$$z_{0_F} = 256 \times 0.00107 = 0.271 \text{ m}$$

$$(z - d)_F = 256 \times 0.215 = 54.4 \text{ m}$$

and from Fig. 4 $L_{x_{u_F}} = 110$ m. Thus the second iteration scale factor is

$$S_2 = L_{x_{u_F}}/L_{x_{u_M}} = 273.$$

After the third iteration $S_3 = 278$, and the fourth iteration gives no change in last figure, thus the scale factor by graphical iteration is $S = 278$.

(b) Deterministic approach

The deterministic approach uses the dimensional properties of the ESDU [2] empirical equation for L_{x_u}. Replacing each full-scale parameter by the product of the scale factor and the model-scale value gives

$$SL_{x_{u_M}} = 25[S(z - d)_M]^{0.35} [Sz_{0_M}]^{-0.063} \text{ metres.}$$

A solution for S is obtained in terms of the model values in metres.

$$S = \frac{91.3\,(z - d)_M^{0.491}}{L_{x_{uM}}^{1.403}\, z_{0_M}^{0.088}}$$

For the typical part-depth simulation at $z_M = 0.244$ m, inserting the model value yields

$$S = \frac{91.3 \times 0.215^{0.491}}{0.403^{1.403} \times 0.00107^{0.088}} = 280$$

The difference in the scale-factor value determined from the same data by each method reflects the inaccuracies inherent in the graphical-iteration method through the reading-off of values from graphs. The deterministic method is to be preferred, being more precise and convenient to use, but is possible

only because the ESDU empirical equation is easily soluble for S. Counihan [3] suggests a different form which is not as amenable, although the graphical iteration method may still be applied successfully.

As the parameter L_{x_u} is a function of height, the process should be repeated at intervals through the depth of the simulation. The reader is invited to confirm that the data for L_{x_u} at $z_M = 0.122$ m in Fig. 7 result in a scale-factor estimate of $S = 277$. The useful height range of a part-depth simulation may be determined by repeating the scaling process at increasing heights until the scale factor alters significantly in value.

5. Comparison of other model flow properties with design values

Once the scale factor has been estimated, the reference model windspeed can be related to the model windspeed at the height equivalent to the meteorological standard of 10 m ($U_{10}/U_{ref} = 0.604$ for the typical part-depth simulation), whence the model data can be compared with the design curves. The mean velocity profile and the u-component spectrum (Figs. 6—8) are fitted to the design data as part of the scaling method. Of the major flow parameters, those remaining to be checked are the variation with height of the three turbulence component intensities and the Reynolds stress, and also the v- and w-component spectra. Figure 9 shows the intensity and Reynolds stress data of the typical part-depth simulation plotted onto the design curves at a scale factor of 280. The comparisons may be extended to include co-variances, cross-spectra etc., limited only by the availability of suitable full-scale data. However, it is suggested that the comparisons shown are sufficient for most applications.

6. Concluding remarks

Owing to the functional dependence of L_{x_u} on z_0 and $(z - d)$, a model boundary layer will have a unique scale factor. The linear scale of any building model should be matched to this scale factor, otherwise the scales of the simulated atmospheric turbulence and the building-generated turbulence will not match. In that event, the scaled dynamic response of the model in load or in deflection will not be correct.

One criticism of the part-depth simulation approach [6] is that since the integral lengths of turbulence in the boundary layer as a whole are related to the depth, partial models 'undoubtedly' underestimate them. The main advantage of a part-depth simulation is that of achieving an adequate model

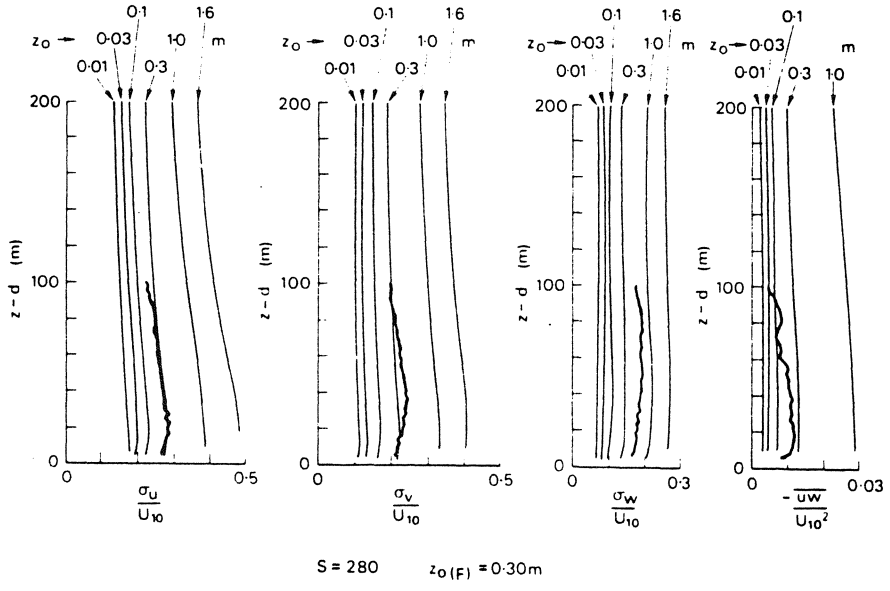

Fig. 9. Turbulence intensity and Reynold stress data for typical part-depth simulation.

size for low-rise buildings. Although the maximum integral length is indeed a function of boundary-layer depth, this maximum occurs above 200 m. The integral lengths near the ground are more closely related to the height above ground. Since the integral length L_{x_u} is specifically matched by the scaling process described, the criticism is insubstantial, providing the match is made over a sufficient depth compared with the height of the building model.

The equivalent full-scale roughness parameter of the part-depth simulation used to illustrate the scaling process is $z_0 = 0.30$ m, corresponding to sub-urban development. The fit of the data to the design curves in Fig. 9 is open to some criticism, particularly in respect of the decreasing Reynolds stress with height and the excessive w-component intensity, but this is the fault of the particular simulation and not of the scaling process.

Acknowledgement

The work described has been carried out as part of the research programme of the Building Research Establishment of the Department of the Environment and this paper is published by permission of the Director.

Nomenclature

α exponent in power law $U/U_{\text{ref}} = (z/z_{\text{ref}})^{\alpha}$
d zero-plane displacement in law-of-the-wall $U = (u_*/\kappa)\ \ln\ [(z - d)/z_0]$
F power spectral density
κ Von Karman constant = 0.40
L_x longitudinal integral length parameter
n frequency
ρ auto-correlation coefficient
S scale factor
σ root-mean-square intensity
t time
τ_0 surface shear stress
U mean velocity
u_* friction velocity in law-of-the-wall
u streamwise turbulence component
v cross-wind turbulence component
w vertical turbulence component
z height above ground
z_0 roughness length parameter in law-of-the-wall

Subscripts: any of the above used as subscript denotes variable of which subscripted parameter is a property. Otherwise: ref denotes reference value, 10 denotes value at 10 m height full scale, M denotes model-scale value, F denotes full-scale value.

{ } type of brackets denote functional dependence on parameters within.

References

1 Characteristics of windspeed in the lower layers of the atmosphere near the ground: strong winds (neutral atmosphere). ESDU Data Item No 72026, Engineering Sciences Data Unit, London, 1972.
2 Characteristics of atmospheric turbulence near the ground. ESDU Data Items Nos 74030, 74031, 75001, Engineering Sciences Data Unit, London, 1974, 1975.
3 J. Counihan, Adiabatic atmospheric boundary layers: A review and analysis of data from the period 1880—1972. Atmos. Envir., 9 (1975) 871—905.
4 N.J. Cook, On simulating the lower third of the urban adiabatic boundary layer in a wind tunnel. Atmos. Environ., 7 (1973) 691—705.
5 R.A. Antonia and R.E. Luxton, The response of a turbulent boundary layer to a step change in surface roughness. Part 1. Smooth to Rough. J. Fluid Mech., 48 (1971) 721—761.
6 N. Isyumov and A.G. Davenport, The ground level wind environment in built-up areas. Proc. 4th Int. Conf. Wind Effects on Buildings and Structures, Heathrow, 1975, Cambridge University Press, London, 1977, pp. 403—422.

(184) Dd0531050 2,200 2/79 HPLtd So'ton G3927